Available online at www.sciencedirect.com
SCIENCE DIRECT®
Journal of Nuclear Materials 348 (2006) 114–121
journal of nuclear materials
www.elsevier.com/locate/jnucmat

Phase diagram of the ZrO_2–FeO system

S.V. Bechta [a,1], E.V. Krushinov [a,2], V.I. Almjashev [b,3], S.A. Vitol [a,4], L.P. Mezentseva [b,*], Yu.B. Petrov [c,5], D.B. Lopukh [c,6], V.B. Khabensky [a,7], M. Barrachin [d], S. Hellmann [e], K. Froment [f], M. Fischer [e], W. Tromm [g], D. Bottomley [h], F. Defoort [f], V.V. Gusarov [b,8]

[a] *A.P. Aleksandrov Research Institute of Technology, Sosnovy Bor 188540, Russia*
[b] *Institute of Silicate Chemistry of Russian Academy of Sciences, nab. Makarova, 2, Saint-Petersburg 199034, Russia*
[c] *Saint-Petersburg Electrotechnical University 'LETI', prof. Popova str., 5, Saint-Petersburg 197376, Russia*
[d] *Institut de Radioprotection et Sûreté Nucléaire (IRSN), BP 3 F-13115 St Paul Lez Durance, France*
[e] *Framatome ANP GmbH, Freyeslebenstr. 1, 91058 Erlangen, Germany*
[f] *Laboratoire de Physico-chimie et Thermohydraulique Multiphasiques (LPTM), CEA/Grenoble, DTN/SE2T/LPTM – 17 rue des Martyrs, 38 054 Grenoble cedex 9, France*
[g] *FZK, IKET, Karlsruhe, Forschungszentrum Karlsruhe GmbH, P.O Box 3640, D-76021 Karlsruhe, Germany*
[h] *European Commission – DG – Joint Research Centre, Institute for Transuranium Elements, Postfach 2340, Hermann-von-Helmholtz Pl. 1, 76125 Karlsruhe, Germany*

Received 9 June 2005; accepted 19 September 2005

Abstract

The results on the ZrO_2–FeO system studies in a neutral atmosphere are presented. The refined eutectic point has been found to correspond to a ZrO_2 concentration of 10.3 ± 0.6 mol% at 1332 ± 5 °C. The ultimate solubility of iron oxide in zirconia has been determined in a broad temperature range, taking into account the ZrO_2 polymorphism. A phase diagram of the pseudobinary system in question has been constructed.

PACS: 81.40.−z; 64.90.+b; 64.70.Dv

* Corresponding author. Address: ul. Karbysheva, d. 10, kv.108, 194021 Saint-Petersburg, Russia. Tel.: +7 812 328 85 91; fax: +7 812 328 85 89.
E-mail address: la_mez@mail.ru (L.P. Mezentseva).
[1] Address: ul. Krasnykh Fortov, d. 27, kv. 19, Sosnovy Bor 188540, Russia.
[2] Address: prospect Al. Nevskogo, d. 21, Sosnovy Bor 188540, Russia.
[3] Address: ul. Aviakonstructorov, d. 24, kv. 173, Saint-Petersburg 197373, Russia.
[4] Address: prospect Geroev, d. 5, kv. 180, Sosnovy Bor 188540, Russia.
[5] Address: ul.Burceva, d. 19, kv. 25, Saint-Petersburg 198261, Russia.
[6] Address: ul. Kuibysheva, d. 23, kv. 44, Saint-Petersburg 197046, Russia.
[7] Address: Socialist st., d. 1/32, kv.-3, St Petersburg 191119, Russia.
[8] Address: ul. Frunze, d. 23, kv. 34, Saint-Petersburg 196135, Russia.

0022-3115/$ - see front matter
doi:10.1016/j.jnucmat.2005.09.009

1. Introduction

A better knowledge of phase equilibria at high temperatures in the (U–Zr–Fe–O)-type corium system is expected to improve the quality of modeling of (1) the molten pool structure and the behavior during Nuclear Power Plant (NPP) severe accidents involving core melting, (2) thermal and physicochemical processes occurring at the interaction of oxidic and metallic melt components, and (3) corium interaction with the structures surrounding the pool. The intensive development of theoretical methods of phase diagram calculation and their application in modeling of severe accident phenomena is currently underway. These efforts have resulted in various numerical codes [1], such as GEMINI [2], MULTICOM [3,4] and code-oriented databases like IVTANTHERMO [5] and NUCLEA [6,7]. The validation of phase diagram databases requires experimental support focused on studying the still unexamined systems or domains (at high temperatures, as a rule) and refining the available data.

The understanding of these processes requires experimental support focused on studying these still unexamined systems. Owing to the EU support, in recent years the work on NPP safety, and phase diagram investigations in particular, have been integrated into large international projects like CIT (Corium Interaction and Thermochemistry), ENTHALPY (European Nuclear Thermodynamic Database validated and applicable in Severe Accidents) and ISTC (International Science and Technology Center) projects. The results offered in the present paper have been obtained within the ISTC 'CORPHAD' project (CORium PHAse Diagrams for multicomponent corium systems and products of its interaction with NPP materials).

It should be noted that the importance of the described work, in principle, goes beyond the scope of NPP severe accident research, as iron oxides and zirconia are important components of many inorganic materials. Special interest in the zirconia-containing systems is explained by their highly refractory nature, strength, crack-resistance, chemical inertia, superionic conductivity for oxygen and other important properties of ZrO_2-based materials [8]. Besides, ZrO_2 and FeO are basic components of the systems which are important as refractories for retaining metallurgical slags [9].

The investigation of phase equilibria in the ZrO_2–FeO system still requires a number of methodological problems to be overcome and due to this the system has been little studied. First of all, the ZrO_2–FeO phase diagram is complicated by ZrO_2 polymorphism at high temperatures. Three structural modifications of zirconia exist in the system at different temperatures under normal pressure, namely monoclinic (m-ZrO_2), tetragonal (t-ZrO_2) and cubic (c-ZrO_2) [10]. The transformation temperatures of m-ZrO_2 → t-ZrO_2 and t-ZrO_2 → c-ZrO_2 are 1172 and 2347 °C, respectively, while the melting temperature is 2710 °C [5]. Besides, the influence of the oxygen partial pressure on the phase state and composition of the iron-containing phases [11–16] also considerably complicates phase equilibria investigations in this system.

The analysis of data from a periodical multivolume reference book on phase diagrams [17] has shown that only one work devoted to the ZrO_2–FeO phase diagram studies is currently known. The system has been investigated by Fischer and Hoffmann [18] at relatively low temperatures up to 1800 °C. The determined eutectic point corresponded to a ZrO_2content of 1.8 mol% at 1330 ± 15 °C; the region of ZrO_2-based solid solutions (SS) was up to 6.7 mol% FeO at 1450 °C and 5 mol% FeO at 1800 °C. Also, these SS were subjected to X-ray diffraction (XRD) and the unit-cell parameters of the ZrO_2-based SS were determined [18].

2. Materials and methods

The initial substances for specimen preparation were as follows: ZrO_2 (>99.3 mass% purity) and FeO as a reagent with a content of (FeO + Fe_2O_3 + Fe) > 98.5 mass%. The specimens of the ZrO_2–FeO system were produced in the 'Rasplav 2' and 'Rasplav 3' facilities by the method of induction melting in a cold crucible (IMCC) under flowing argon [19–21]. In order to crystallize iron oxide as a wüstite structure ($Fe_{1-x}O$) with a certain composition that would be the closest to the FeO stoichiometry ($Fe_{0.947}O$), pure metallic iron (Fe > 99.9 mass% purity) was added to the initial mass and as a getter in the quantity of 1 mass% over the total mass. It should be noted that such a quantity of iron in the system has practically no influence on the liquidus temperature of the ZrO_2–FeO system due to low solubility of iron in an oxidic melt.

The phase composition of the specimen was measured by XRD using the DRON-3 X-ray diffractometer with the CoK_α radiation.

The chemical composition of the specimen was determined by spectrophotometric and gas volumetric

analyses [22–24] as well as by X-ray fluorescence (XRF) using the SPARK 1-M spectrometer.

The microstructure of the specimen, its elemental composition and the composition of separate phases were analyzed by means of scanning electron microscopy (SEM) and energy-dispersive X-ray spectrometry (EDX) using the CamScan MV2300 or ABT-55 coupled with the Oxford Link microprobe analyzer. The error in determining the elements content by this method varies with the atomic number and equals to ±0.3 mass% on average.

Thermal transformations in the system were studied by differential thermal analysis (DTA) using the SETARAM TAG-24 and NETZSCH STA 429 thermal analyzers. Temperature values of the thermal effects were determined from the corresponding peak onset in the DTA curves. The peak onset point was identified from the intersection of the tangents extrapolated from the baseline and the thermal effect curve. The DTA tests were carried out with specimens weighing about 30 mg, heated with the rate of 10 °C/min in a neutral atmosphere (argon or helium). However, the above methods of thermal analysis were found to be applicable for the system only in a very limited range of temperatures and compositions because of the melt interaction with practically all tested crucible materials (Al_2O_3, ZrO_2, W, W/Re, Ir, etc.). Therefore, the determination of solidus (T_{sol}) and liquidus (T_{liq}) temperatures for the majority of compositions was carried by the method of visual polythermal analysis (VPA) using the original facilities: 'Rasplav 2&3' designed for induction melting in the cold crucible (VPA IMCC, Fig. 1(a)) [20] and the Galakhov microfurnace (Fig. 1(b)) [25].

For the T_{liq} determination by VPA IMCC, the molten pool surface temperature was measured by

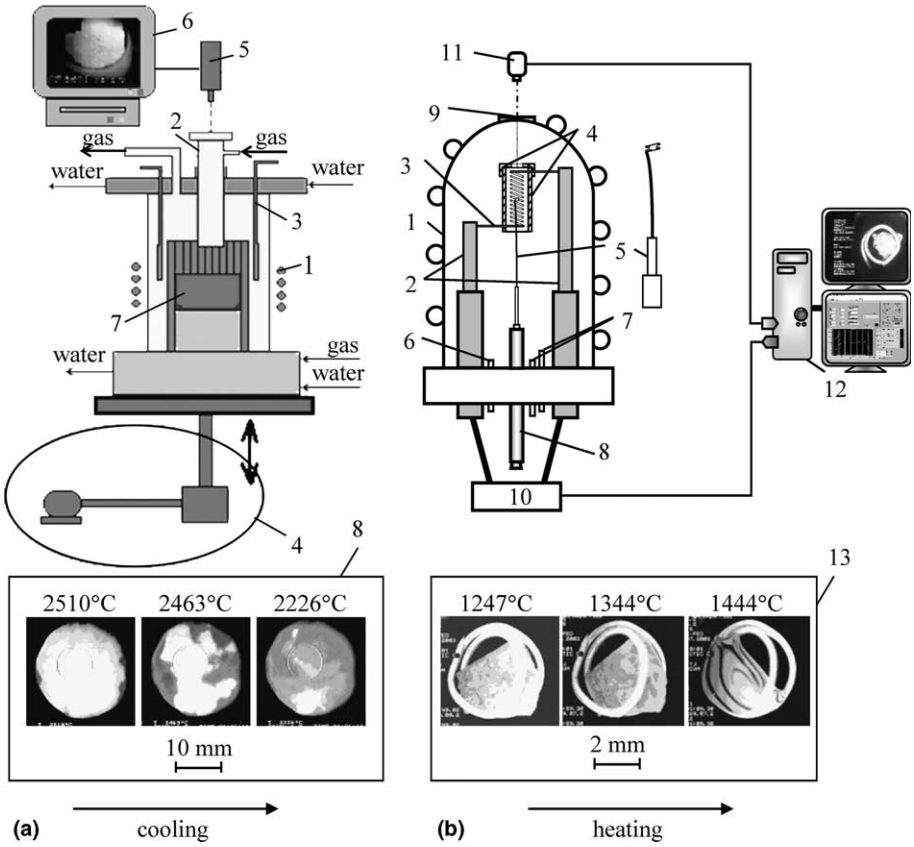

Fig. 1. Schematics of visual polythermal analysis facilities: (a) Induction melt in cold crucible facility 'Rasplav 3': 1 – inductor, 2 – pyrometer shaft, 3 – movable water-cooled electromagnetic screen, 4 – crucible vertical shift drive, 5 – pyrometer coupled with a videocamera, 6 – control and registration system, 7 – melt, 8 – cooling molten pool surface in the sighting spot; and (b) Galakhov microfurnace: 1 – water-cooled sealed body, 2 – steel electrodes, 3 – tungsten heating coil, 4 – molybdenum protective screens, 5 – specimen holder (iridium or molybdenum), 6 – pumping-out system, 7 – gas flooding system, 8 – specimen quenching device, 9 – quartz viewing port, 10 – regulated power sources, 11 – videocamera, 12 – observation and control system, 13 – view of a specimen in the holder during heating.

the spectral ratio pyrometer at the instant of the solid phase appearance in the pyrometer sighting spot (Fig. 1(a), 8 – middle frame). The appearance of the solid phase nuclei on the locally cooled surface of the volumetrically superheated molten pool was recorded with a high speed digital video camera and the images were subjected to a frame-by-frame analysis. The maximum error of T_{liq} measurement by this method for the compositions with a big $T_{sol} - T_{liq}$ difference is not more than 50–75 °C, but usually the error is significantly smaller. It should be noted that regardless of the compositions and temperatures, the VPA IMCC application ensures the absence of interaction between the crucible materials and the melt and of contamination of the melt by corrosion products. For VPA in the Galakhov microfurnace, fragments of the ingot prepared by IMCC, weighing 7–8 mg each, were taken and fixed between the coils of the holder located in the isothermal microfurnace zone (Fig. 1(b)). The effective range of temperature measurements in the microfurnace is between 900 and 2500 °C with an accuracy of around ±30 °C [25]. The measurements were made in a neutral atmosphere (high-purity helium under 0.25×10^5 Pa (0.25 bar) for the low-temperature domain, an argon–hydrogen mixture, 96 vol.% Ar–4 vol.% H_2, under 1.25×10^5 Pa (1.25 bar) for the high-temperature domain). To avoid active interaction between the specimen and the holder, the latter was produced from iridium. Moreover the possible effect of the heating rate on the error of visual determination of the melting initiation temperature and the complete melting was checked and the optimal rate of 5 °C/s was chosen near the critical points. The process of specimen melting was recorded with a digital video camera and the images subjected to a frame-by-frame analysis. T_{sol} was defined as the temperature at which sharp edges of the specimen started degrading during heating. T_{liq} was defined as the temperature of the specimen's complete spreading across the holder (Fig. 1(b), 13 – last frame). The microfurnace design allows quenching of specimens by means of dropping them together with the holder into the cold zone of the furnace. After quenching, the microstructure and elemental composition of the phases of the specimen were analyzed.

3. Discussion of results

Table 1 contains the chemical analysis of the specimen's composition after IMCC and the EDX data on the composition after studies in the Galakhov microfurnace. The same table contains T_{sol} and T_{liq} values determined for the ZrO_2–FeO system by VPA IMCC, VPA in the Galakhov microfurnace, and DTA.

Table 1
T_{sol} and T_{liq} in the ZrO_2–FeO system

ZrO_2 content, mol%	Temperature, °C	
	Solidus	Liquidus
10.3[a]	1332[b]	1347[b]
13.7[a]	–	1591[c]
14.5[d]		1605[e]
19.7[a]		1797[c]
21.4[d]		1793[e]
31.6[a]		2040[c]
33.2[d]	1342[c]	2030[e]
33.6[d]	–	2020[e]
42.0[d]		2112[e]
44.8[d]		2161[e]
49.7[a]		2146[c]
58.7[a]		2331[c]
71.2[d]		2463[e]

[a] EDX.
[b] DTA.
[c] VPA in the Galakhov microfurnace.
[d] Chemical analysis data.
[e] VPA IMCC.

Since the melt resulting from heating the specimens wetted easily all the crucible materials, interacted with oxide materials and which then flowed out of the crucible in substantial quantities, only DTA allowed a reliable determination of the eutectic temperature (T_{eut}). Fig. 2 presents a thermogram

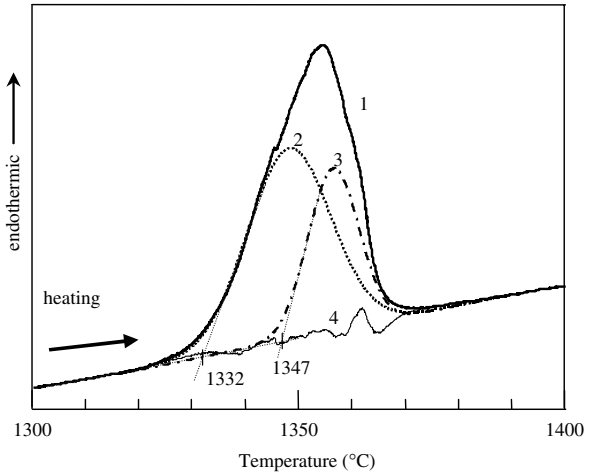

Fig. 2. DTA curve for ZrO_2–FeO system specimen containing 10.5 mol% ZrO_2 in neutral atmosphere: 1 – experimental curve; 2 and 3 – peak breakdown 1; 4 – difference between curve 1 and the sum of curves 2 and 3.

for the specimen containing 10.5 ± 0.5 mol% ZrO_2 in platinum crucible. The DTA data analysis shows this specimen to have a composition close to the eutectic. At the same time, the possibility of the endothermal peak interpretation as two overlapping endothermal effects (Fig. 3, Table 1) indicates some deviation from the eutectic point in the specimen's composition. The difference between T_{sol} and T_{liq} for this composition was 15 °C. The first of the two overlapping thermal effects, observed at 1332 °C, corresponds to the eutectic temperature of the system. The second one, observed at 1347 °C, is related to the deviation from the eutectic composition.

The X-ray pattern of this sample has shown that the system represents a mixture of the wüstite-type iron oxide ($Fe_{0.947}O$) and t-ZrO_2(FeO) SS (Fig. 3(a)).

Since the specimen with a composition close to the eutectic contains very small crystals of the ZrO_2-based phase (Fig. 4(a)), the employment of EDX for determining the FeO concentration would have lead to overestimating the iron oxide content in the SS. Therefore, in order to determine the solubility limit of FeO in the ZrO_2-based phase more precisely, the SEM/EDX analysis was carried out on the specimen regions containing sufficiently large grains of the ZrO_2-based phase which had formed through the solid phase recrystallization at a temperature close to the eutectic (Fig. 4(b), Table 2). According to the EDX results for these regions, the maximum FeO content in the ZrO_2-based SS at practically T_{sol} (1330 °C) is about 2.2 mol% (Fig. 4(b), Table 2, region 2). The EDX analysis of the FeO-based phase from the same specimen has shown an insolubility of zirconia in this phase (Fig. 4(a) and Table 2, region 1).

The phase corresponding to the ZrO_2-based SS was found practically in all specimens (e.g. Fig. 4(c), Table 2, region 4). However, in the majority of the crystallized specimens the SS grains were too small for the precise determination of their composition by EDX. In order to determine the FeO SS content in ZrO_2, an additional test has been performed. It was aimed at growing a layer of the ZrO_2(FeO) SS by drawing the crucible with the melt out of the inductor at 8–10 mm/h for 1 h at 2030 °C of the molten pool surface. A composition of 33.2 mol% ZrO_2 was used in the test. Owing to the thickness of the layer produced by the ZrO_2(FeO) SS crystallization, more precise data on the FeO ultimate solubility in ZrO_2 could be obtained (Fig. 4(d), Table 2, region SQ3).

The XRD analysis of a specimen containing 33.2 mol% ZrO_2 revealed the presence of FeO in the form of wüstite and of the Zr(Fe)O_2-based SS in the cubic form (Fig. 3(b)). To study the SS more thoroughly, the specimen was washed with concentrated hydrochloric acid to remove the FeO phase. The X-ray pattern of the resulting specimen (Fig. 3(c)) shows the presence of two phases, namely the prevailing c-ZrO_2(FeO) SS, and a small quantity of m-ZrO_2 (marked as I^1 and I^2).

A calculation of the cubic SS to monoclinic SS ratio by the formula from Ref. [26] shows the

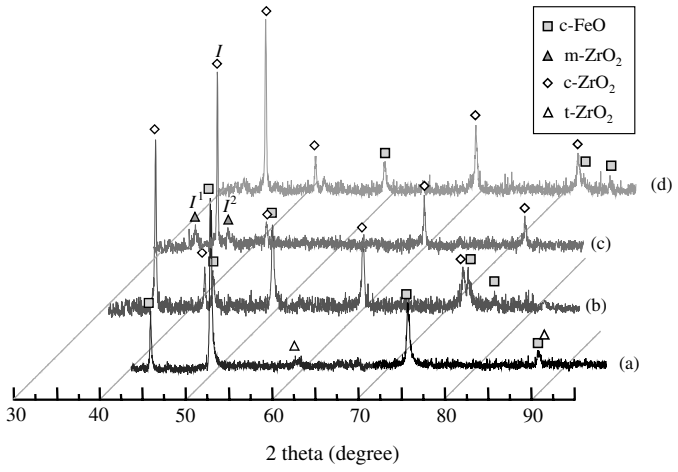

Fig. 3. X-ray patterns of the ZrO_2–FeO system specimens with different zirconia content: (a) 10.3 mol% ZrO_2 cooled slowly through 1330 °C; (b) 33.2 mol% ZrO_2 quenched from 2030 °C; (c) FeO SS in ZrO_2, quenched from 2030 °C (FeO-based phase washed out from specimen); and (d) 58.7 mol% ZrO_2, quenched from 2300 °C; I^1 – c-ZrO_2(FeO) SS and I^2 – m-ZrO_2.

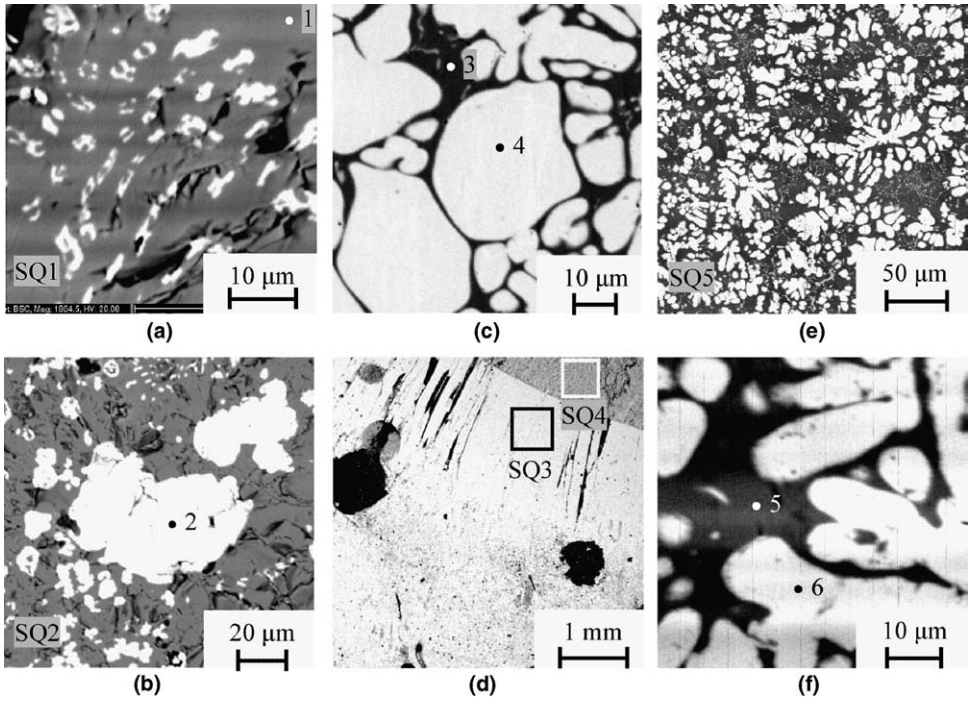

Fig. 4. Micrographs of the crystallized ZrO_2–FeO specimens with different zirconia content: (a, b) 10.3 mol% ZrO_2–eutectic composition cooled slowly through 1330 °C; (c) 33.2 mol% ZrO_2, quenched from 2030 °C; (d) 33.2 mol% ZrO_2 obtained by drawing ingot out from inductor; and (e, f) 58.7 mol% ZrO_2 quenched from 2300 °C.

(c-ZrO_2 + m-ZrO_2) mixture to contain about 70 relative% of c-ZrO_2. The monoclinic ZrO_2 may possibly be due to partial decomposition – during the ingot cooling – of the fine-grained c-Zr(Fe)O_2 SS with iron oxide separation followed by the c-ZrO_2 → t-ZrO_2 → m-ZrO_2 transformations.

On the basis of the chemical analysis and XRF data for the specimen, and taking into consideration that practically all iron oxide was in the form of the c-ZrO_2(FeO) SS (Fig. 3(c)), and allowing for the fractionation of c-ZrO_2 into a c-ZrO_2 + m-ZrO_2 mixture, the content of FeO in c-ZrO_2(FeO) is evaluated at 10.5 mol%. It should be noted that the obtained value agrees well with the data in Table 2 (region 4) and SQ3 in Fig. 4(d).

Table 2
Chemical analysis data for the regions marked in Fig. 4

ZrO_2 content in specimen, mol%	Examined region	Components content, mol%	
		ZrO_2	FeO
10.3	1	–	100
	2	97.8	2.2
	SQ1	10.3	89.7
	SQ2	10.2	89.8
33.2	3	–	100
	4	88.3	11.7
	SQ3	87.1	12.9
	SQ4	31.6	68.4
58.7	5	–	100
	6	90.5	9.5
	SQ5	58.4	41.6

The specimen with 58.7 mol% ZrO_2, which had been quenched from T_{liq} (2300 °C), was subjected to the SEM/EDX and XRD analyses at room temperature. The microstructure and composition data for the crystallized phases are given in Fig. 4(e) and (f) and Table 2. From the X-ray pattern of the specimen (Fig. 3(d)) it follows that from 2300 °C the ZrO_2-based SS crystallizes in the cubic modification, as with the specimen containing 33.2 mol% ZrO_2.

Table 3 contains unit cell parameters of the cubic and tetragonal ZrO_2-based SS measured at room temperature. The analysis of the data from Table 3 shows that the unit-cell parameters and cell volume somewhat decrease as the FeO content increases in the c-Zr(Fe)O_2 SS.

On the basis of the composition, T_{sol} and T_{liq} data obtained by different methods (Tables 1 and 2), and the structure of the ZrO_2-based

Table 3
Structural characteristics of ZrO_2(FeO) SS

FeO content in ZrO_2-based SS, mol%	Structure	Unit cell parameters, nm	Unit cell volume, nm^3
2.2[a]	Tetragonal	$a = 50.7 \pm 0.2$ $c = 51.7 \pm 0.3$	$(132.8 \pm 1.4) \times 10^3$
0 (17-923)[b]		$a = 51.2$ $c = 52.5$	137.63×10^3
11.3 ± 0.5[a]	Cubic	$a = 50.85 \pm 0.6$	$(131.4 \pm 0.5) \times 10^3$
10.5[c]		$a = 50.9 \pm 0.4$	$(132 \pm 3) \times 10^3$
9.3 ± 0.2[a]		$a = 50.8 \pm 0.1$	$(131 \pm 1) \times 10^3$
0 (27-997)[b]		$a = 50.9$	$(132.97) \times 10^3$

[a] EDX (Table 2).
[b] ASTM file data.
[c] Chemical analysis of specimen with FeO-based phase washed out.

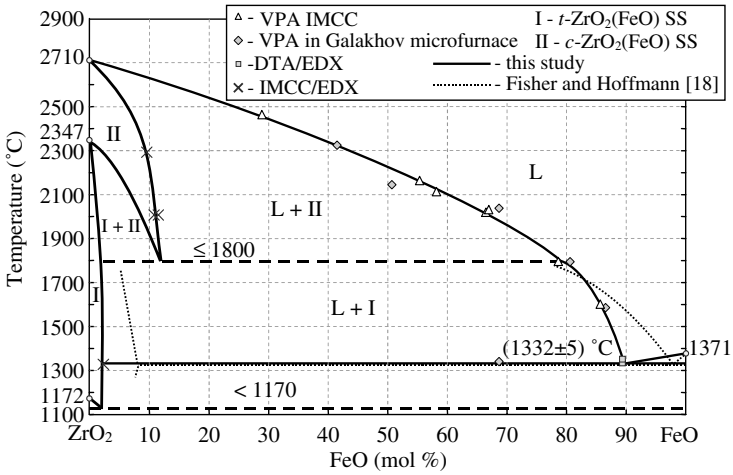

Fig. 5. Phase diagram of the ZrO_2–FeO system.

phases, a phase diagram of the ZrO_2–FeO system has been constructed (Fig. 5). The values of T_{sol} and T_{liq} determined by the different methods are quite similar, and thus indicate that the results are reliable.

The liquidus curve behavior, the data of the DTA (Fig. 2) and SEM/EDX analyses (Fig. 4(a); Table 2, SQ1 region) indicate that the eutectic point in the ZrO_2–FeO system corresponds to the ZrO_2 content of 10.3 ± 0.6 mol% at 1332 ± 5 °C. It should be stressed that the values of the eutectic composition concretely differ from those given in [22] where it was indicated as only 1.8 mol% ZrO_2 (Fig. 5).

Though, the c-ZrO_2(FeO) SS has been recorded in many tests, more refined data for the temperature along the lower boundary of its existence are still required. The kink in the liquidus line of the ZrO_2–FeO system suggests that the temperature of the zirconia-based cubic SS → tetragonal SS transformation is not higher than 1800 °C. The iron oxide solubility in m-ZrO_2 must be very low because neither EDX nor the unit-cell determination during the specimens XRD analysis could register any solubility. This finding corroborates the results given in [18].

4. Conclusions

A pseudobinary phase diagram of the ZrO_2–FeO system in an inert atmosphere (Ar) has been constructed. The diagram has a eutectic point and a phase region of FeO solid solution in ZrO_2. The eutectic composition and temperature in the system have been specified. They correspond to 10.3 ± 0.6 mol% of ZrO_2 and 1332 ± 5 °C.

The parameters of the FeO solid solution in ZrO_2 have been determined as follows:

t-ZrO_2(FeO) exists in the temperature range from 1172 to 2347 °C, the ultimate FeO solubility in t-ZrO_2 is 2.2 ± 0.3 mol% at 1332 °C;
c-ZrO_2(FeO) exists in the temperature range of approximately 1800 °C (or less) up to 2710 °C, the solubility limit of FeO in ZrO_2 at 1800 °C is about 13 mol% FeO.

Acknowledgments

The present work has been carried out within the framework of the ISTC Project #1950.2 financed by the EU. The authors express their gratitude to Dr A. Zurita, Professor L. Tocheny and Dr V. Rudneva acting in the capacity of research coordinators from the EC and ISTC, and to Dr Yu. Aniskevich, the Project Manager. Also, the authors would like to thank Dr G. Cognet and Dr B. Adroguer for their valuable comments and suggestions made when planning the work and discussing the results at the annual project meetings.

References

[1] G.V. Belov, Thermodynamic Modeling: Methods, Algorithms, Software, Nauchny Mir Publishers, Moscow, 2002 (in Russian).
[2] B. Cheynet, P.Y. Chevalier, E. Fischer, CALPHAD 26 (2002) 167.
[3] V.I. Almyashev, V.V. Gusarov, O.V. Mazurin, in: Proceedings of a Scientific and Practical Workshop on 'New Achievements in Chemistry and Materials Technology', St. Petersburg, 2002, p. 62 (in Russian).
[4] O.V. Mazurin, V.V. Gusarov, Phys. Chem. Glass 28 (2002) 74 (in Russian).
[5] G.V. Belov, V.S. Iorish, V.S. Yungman, CALPHAD 23 (1999) 173.
[6] P. Chaud, P.Y. Chevalier, B. Cheynet, E. Fischer, P. Mason, M. Mignanelli, NUCLEA Database developed by THERMODATA/INPG/CNRS and AEA-T, Contributions in Final ENTHALPY Report, ENTHA(03)-P018, European Commission, 5th Framework Program, Nuclear Fission, 2000–2003.
[7] P.Y. Chevalier, E. Fischer, B. Cheynet, CALPHAD 28 (2004) 15.
[8] L.G. Nekhamkin, Yu.A. Tsylov, M.N. Butova, et al., in: Production of Rare Metals and Semiconductor Materials. Review. Issue 1, TsNIITsvetMet Publishers, Ioscow, 1989, p. 25 (in Russian).
[9] S.I. Filippov, S.P. Arsenyev, V.V. Yakovlev, et al., Physico-Chemical Methods in Studies of Metallurgical Processes, Metallurgiya Publishers, Moscow, 1968 (in Russian).
[10] V.A. Rabinovich, Z.Ya. Khavin, Brief Chemical Reference Book, 2nd Ed., Revised and Updated., Chemistry Publishers, Leningrad, 1978 (in Russian).
[11] L.S. Darken, R.W. Gurry, J. Am. Chem. Soc. 67 (1945) 1398.
[12] L.S. Darken, R.W. Gurry, J. Am. Chem. Soc. 68 (1946) 798.
[13] P.E.C. Bryant, W.W. Smeltzer, J. Electrochem. Soc. 116 (1969) 1409.
[14] O. Kubaschewski, Iron – Binary Phase Diagrams, Springer-Verlag, Berlin, 1982.
[15] P.T. Carter, M. Ibrahim, J. Soc. Glass Technol. 36 (1952) 142.
[16] N.A. Toropov, V.P. Barzakovsky, I.A. Bondar, et al. Handbook, Issue 2, Metal-Oxygen Compounds of Silicate Systems, Nauka Publishers, Leningrad, 1969 (in Russian).
[17] N.A. Toropov, V.P. Barzakovsky, V.V. Lapin, N.N. KurtsevaReference Book, Issue 1, Binary Systems, Nauka Publishers, Moscow, Leningrad, 1965 (in Russian).
[18] W.A. Fischer, A. Hoffmann, Arch. Eisenhütt. 28 (1957) 739.
[19] Yu.B. Petrov, Induction Melting of Oxides, Energatomizdat Publishers, Leningrad, Leningrad Branch, 1983 (in Russian).
[20] D. Lopukh, S. Bechta, A. Pechenkov, et al., in: Proceedings of ICONE 8 of 8th International Conference on Nuclear Engineering, Baltimore, Maryland, USA, 2–6 April 2000, ICONE-8139.
[21] L.M. Viting, High-Temperature Solutions and Melts, Moscow State University Publishers, Moscow, 1991 (in Russian).
[22] GOST 4011-72. Drinking Water. Methods of Measuring Mass Concentration of Total Iron (in Russian).
[23] E.B. Sandell, Colorimetric Determination of Traces of Metals, Mir Publishers, Moscow, 1964 (in Russian).
[24] B.G. Yeremina, Gas Analysis, Goskhimizdat Publishers, Leningrad, 1955 (in Russian).
[25] F.Ya. Galakhov, in: Modern Techniques of Silicate and Construction Materials Studies, Gosstroyizdat Publishers, Moscow, 1961, p. 178 (in Russian).
[26] O.V. Pozhidayeva, E.N. Korytkova, I.A. Drozdova, V.V. Gusarov, J. Gen. Chem. (Zhurnal obshchei khimii) 69 (1999) 1265 (in Russian).